Wavelets, Local Tomography and Interventional X-Ray Imaging

Anne Bilgot, Valérie Perrier, and Laurent Desbat

***Abstract*— Interventional reconstruction of tomographic sections is still a challenging task: interventional scanners obstruct the operative field, and CT-assisted surgical acts are known to be irradiant. An alternative consists in using a C-Arm fitted out with a digital detector for X-Ray data acquisition, but one has then to cope with the limited size of the existing detectors: they are not wide enough to collect the whole beam emerging from a section, and thus prevent from applying conventional reconstruction techniques. The work we present here relies on such an architecture, and aims at applying local tomography principles to this context: when only X-Ray projections through a central section of a larger one are available, one refers to the interior problem, for which it is known that the density of the central section is then not recoverable, but surfaces of discontinuity between anatomical surfaces are theoretically accessible. We propose an implementation of a wavelet-based approach of this problem inspired by a work by Holschneider, where it is proved that the Radon Transform is nothing but a wavelet transform for a well chosen analysis "wavelet". Numerical tests show that our approach supplies reconstruction results from local measurements preserving discontinuities.**

***Index Terms*— Radon transform, Local Tomography, Wavelets.**

I. Background: Interventional Image Reconstruction

ALTHOUGH Computed-Tomography scanners have now entered the operating room, interventional reconstruction of tomographic sections remains a challenging task: such devices obstruct the operative field, and CT-assisted surgical acts are known to be irradiant, in particular for the surgeon's hands. An alternative consists in doing *fluoroscopy-based reconstruction*, for which X-Ray data are acquired using a C-Arm. This X-Ray imaging device is conventional in the operating room and much more ergonomic than a CT scanner; furthermore, it can nowadays be fitted with a digital, and so distortion-free, X-Ray detector. A major drawback in this approach is the might-be presence of radio-opaque objects in the operative field, which truncate projection data (see [1]). Another one - the one we tackle here- lies in the size of the detectors that can be manufactured today: they are likely to be not wide enough to collect the whole beam emerging from a section of a patient lying at the isocenter of the C-Arm. This lack of data prevents from applying conventional CT-reconstruction techniques, and the fact is that existing fluoroscopy-based reconstruction devices only enable to handle small section structures, such as wrists or ankles.

One of the objectives of the European MI3 project, within which this work comes, was to design reconstruction techniques tied to this truncated data context. A C-ARM, in which a digital Pixium 4700 detector (Trixell) is integrated, is used and coupled with a software platform (Surgetics Station, Praxim): once a *reconstruction* is performed (see later), it is possible to navigate inside it all the intervention long, by tracking tools in the operating field and virtually replacing them into the initial images. Thus, it is no longer compulsory to reiterate irradiation all the intervention long.

We are addressing here the reconstruction step: as said before, only truncated data, and more precisely only X-Ray projections through a central section of a larger one, are available. This is the interior problem, also known as the interior Radon transform inversion, a particular case of local tomography we describe in next section. It is known that the density of the central section is then not recoverable, but that the discontinuities, *in some sense*, are. Thus, surfaces of discontinuity between anatomical surfaces are theoretically accessible. This kind of information turns out to be relevant for a surgeon assistance in many interventions (for instance in orthopaedics), and constitutes our target in the present paper.

Manuscript received October 29, 2004.

A. Bilgot is with both TIMC-IMAG and LMC-IMAG laboratories (resp. Faculté de Médecine de Grenoble, 38706 La Tronche Cedex, and Domaine Universitaire, BP53, 30041 Grenoble Cedex, France. email: anne.bilgot@imag.fr).
Pr Valérie Perrier is with LMC-IMAG Laboratory
(email: valerie.perrier@imag.fr).
Pr Laurent Desbat is with TIMC-IMAG Laboratory
(email: laurent.desbat@imag.fr).

II. The Interior Problem

The Radon transform $\mathcal{R}f$ of a function f, supposed to be compactly supported in the unit disk of $\mathbb{R}^2$, is given, along direction $\vec{u_\theta} = (\cos\theta, \sin\theta),\ \theta \in [0, \pi[$, and at distance s from the origin, by

$$\mathcal{R}f(s, \vec{u_\theta}) = \mathcal{R}_\theta f(s) = \int_{t\in\mathbb{R}} f(s\vec{u_\theta} + t\vec{u_\theta}^{\perp})dt$$

where $\vec{u_\theta}^{\perp} = (-\sin\theta, \cos\theta)$ (see Fig.1(a) for illustration).
The Radon transform is inversible through the general Filtered Backprojection formula

$$f \star \mathcal{R}^{\#} e = \mathcal{R}^{\#}(\mathcal{R}f \star e) \tag{1}$$

where $\mathcal{R}^{\#}$ denotes the backprojection operator defined by

$$\mathcal{R}^{\#} g(\vec{x}) = \int_{\theta\in\mathcal{S}^1} g_\theta\,(\vec{x}.\vec{u_\theta})\,d\theta$$

In case of complete data, e is chosen in such a way that $\mathcal{R}^{\#}e$ approximates the Dirac distribution δ up to an implementation cut-off frequency, and e then turns out to be a cut-off ramp filter.

In case of interior data

$$\{\mathcal{R}f(s,\vec{u_\theta}), s \in [-a,a], a < 1, \theta \in [0,\pi[\}$$

(see Fig.1(b) for illustration), this strategy is no longer applicable: the ramp filter is not compactly supported, and the convolution step cannot thus be performed unless all the projections through the whole section are known. Nevertheless, in [2], Natterer proves that the information carried by the interior data are sufficient to identify an approximation of f in the Region Of Interest (ROI) up to a quasi-constant function. Furthermore, Quinto, through microlocal analysis [3], asserts that information on the discontinuities of f in the ROI is available in the truncated projections: it is therefore reasonable to try and reconstruct the discontinuities of f in the context of the interior problem.

The literature gives several approaches to this problem, for instance Λ-*Tomography* (see for instance [4]), where one reconstructs Λf instead of f (the pseudo-differential operator Λ, locally recoverable, is known to preserve the discontinuities) or *Pseudolocal Tomography* [5], where one copes with the non-locality of the ramp filter by truncating it in the direct domain. Another class of methods rely on wavelets or on wavelet-inspired families, such as ridgelets or curvelets (for instance [6] or [**?**]); in particular a key idea is that the 2D wavelet transform of a function f can be computed from a 1D wavelet transform of its Radon transform $\mathcal{R}f$ (e.g. [8]), an approach which can be seen as an another application of (1). The locality of the wavelet filtering thus enables to reconstruct from local data wavelet coefficients of the function f *up to a given scale* (and therefore some well-determined features of f, decomposed in a wavelet basis). The method we present in the following comes within these ideas, but offers a much more simpler way to obtain wavelets coefficients of the Radon Transform.

III. A new local reconstruction method

In [9], Holschneider explains that the Radon Transform is nothing but a wavelet transform for a well chosen analysis tool. Therefore, it is possible to reconstruct f in some wavelet basis, without any additional computation of coefficients. As far as we know, this approach has not yet been implemented in the local tomography context, and this is what we propose here.

As Holschneider did, we consider (following [10]) the 2D directional wavelet transform of $f \in \mathbb{L}^1 \cap \mathbb{L}^2(\mathbb{R}^2)$ against the wavelet $g \in \mathbb{L}^1 \cap \mathbb{L}^2(\mathbb{R}^2)$, defined at scale $a > 0$, at point $\vec{b} \in \mathbb{R}^2$ and along direction given by $\theta \in [0, 2\pi[$ by:

$$\begin{aligned} W^g f(\vec{b},a,\theta) &= < T_{\vec{b}} D_a R_\theta g, f > \\ &= \int_{\vec{t}\in\mathbb{R}^2} f(\vec{t}) \frac{1}{a^2} \bar{g}\left(\frac{r_{-\theta}(\vec{t}-\vec{b})}{a}\right) d\vec{t} \end{aligned}$$

where $T_{\vec{b}}$, D_a and R_θ respectively denote translation, dilatation and rotation operators on $\mathbb{L}^2(\mathbb{R}^2)$, and r_θ the rotation of angle θ in $\mathbb{R}^2$. It is then possible to write the synthesis formula

$$f(\vec{x}) = \frac{1}{c_{gh}} \int_0^\pi \int_{\mathbb{R}^2} \int_{\mathbb{R}_+^*} W_g f(a,\vec{b},\theta)\ T_{\vec{b}} D_a R_\theta h(\vec{x})\ \frac{da}{a^3}\ d\vec{b}\ d\theta$$

provided

$$c_{gh} = 4\pi^2 \int_{\mathbb{R}^2} \frac{\bar{\hat{g}}(\vec{k})\hat{h}(\vec{k})}{\|\vec{k}\|^2} d\vec{k} < +\infty \text{ and } c_{gh} \neq 0$$

(where $\hat{g}$ denotes the Fourier Transform of g, with normalisation $(2\pi)^{-\frac{n}{2}}$ in $\mathbb{R}^n$).

We extend this formalism to the case where g is a tempered distribution (i.e. a distribution on Schwartz space $\mathcal{S}(\mathbb{R}^2)$); hence, by setting

$$g_0 = \delta_{x_1} 1_{x_2} \in \mathcal{S}' : f \in \mathcal{S}(\mathbb{R}^2) \mapsto < g_0, f >= \int_{\mathbb{R}} f(0,x_2) dx_2$$

we get

$$W^{g_0} f(a,\vec{b},\theta) = \frac{1}{a} \mathcal{R}_\theta f(\vec{b}\cdot\vec{u_\theta})$$

and finally

$$f = \frac{1}{c_{g_0 h}} \iiint \frac{1}{a} \mathcal{R}_\theta f(\vec{b}\cdot\vec{u_\theta}) \frac{1}{a^2} h\left(\frac{r_{-\theta}(\vec{x}-\vec{b})}{a}\right) \frac{da}{a^3}\ d\vec{b}\ d\theta \tag{2}$$

provided

$$c_{g_0 h} = 2\pi \int_{k_1\in\mathbb{R}} \frac{\hat{h}(k_1,0)}{|k_1|^2} dk_1 < \infty, \neq 0$$

This condition on the reconstruction wavelet h can be easily fulfilled in practice (for instance with the *mexican hat* (Laplacian of a Gaussian)).

It is then possible to highlight the link between this approach and the traditional algorithm derived from (1), as (2) can be rewritten

$$f(x) = \frac{1}{c_{gh}} \int_\theta \mathcal{R}_\theta f \star \mathcal{R}_\theta H_\theta(\vec{x}.\vec{u_\theta}) d\theta \tag{3}$$

where H_θ, defined by

$$H_\theta(\vec{x}) = \int_{a>0} \frac{1}{a^3} h\left(\frac{r_{-\theta}\vec{x}}{a}\right) \frac{da}{a} \tag{4}$$

gives in fact, after application of the Radon transform, a decomposition scale-by-scale of the ramp filter for each direction θ.

IV. Implementation and Results

Implementation is performed through two steps.

1) The filter H_θ is independant of the function f and thus can be pre-computed. We use the following discretization of (4)

$$H_\theta(\vec{x}) \simeq \ln(a_0) \sum_{\mathtt{j}=\mathtt{scale_{min}}}^{\mathtt{scale_{max}}} \frac{1}{a_0^{3j}} h\left(\frac{r_{-\theta}\vec{x}}{a_0^j}\right)$$

where we have chosen $a_0 = 2^{1/4}$, and where $\mathtt{scale_{min}}$ and $\mathtt{scale_{max}}$ are set according to the range of available

data: in case of complete data, $\texttt{scale}_{\texttt{min}}$ and $\texttt{scale}_{\texttt{max}}$ are given by respectively the resolution and the extent of the support of the image, whereas in case of truncated data, $\texttt{scale}_{\texttt{max}}$ fits the support of available data. Lastly, we use a Laplacian of a Gaussian as reconstruction wavelet h.

2) The reconstruction (3) is computed as a conventional filtered backprojection formula (with a discrete convolution, and then backprojection using a linear interpolation).

A. Reconstruction with global data

We work with a Shepp and Logan Phantom (on the left in Fig. 2(a)). We compare the reconstruction obtained with a conventional Filtered Back-Projection algorithm (FBP) -for which we use Matlab code provided by [11]- with the reconstruction obtained thanks to our method. Results are displayed respectively in the middle and right images in Fig. 2(a). Visually, both reconstructions are of similar quality . To give more insight, we display a comparison of three cross sections (materialized on Fig. 2(b)). These experiments confirm that our algorithm, in case of complete data, provides as satisfactory results as a conventional one (and moreover, it seems that our method suffers less from Gibbs phenomenon).

B. Reconstruction with local data

In this case, a region of interest is defined, together with a bit wider region of exposition. Projections are only computed through the region of exposition, and extended by continuity to the initial support of the Radon Transform (the one of complete projection case).

In order to illustrate the interior problem, we compute the reconstruction of the interior 16-pixel wide region of the phantom, using a 28-pixel wide region of exposition (in red in Fig. 3(a)). Results are displayed in Fig. 3(b): as theorically expected, initial discontinuities are clearly visible in the reconstructed image.

Lastly, we escape from the strictly-defined interior problem and perform the same experiments for an off-centred region: the results displayed in Fig. 3(c) show that we can expect our algorithm to behave successfully in case of other schemes of truncation of data.

V. Conclusion and Perspectives

In this work, a new local inversion formula for the Radon transform using wavelets is implemented. Experiments on a Shepp and Logan phantom show that it behaves well in case of complete projections, and that satisfactory results as regards discontinuities localization are obtained when dealing with local data. Future work will assess properly the performance of our algorithm in comparison with other existing local methods.

Acknowledgment

This work is supported by the Rhône-Alpes Region (AD´eMo grants) and the European Community (IST 1999-12338 MI3 and HPRN-CT 2002-00286 Breaking Complexity grants).

References

[1] X. Liu and M. Defrise and L. Desbat and M. Fleute, *Cone-Beam reconstruction for a C-arm CT system*, Conference Records of the 2001 IEEE Nuclear Science and Medical Imaging Symposium.

[2] F. Natterer, *The mathematics of Computerized Tomography*, Wiley, 1986.

[3] E.T. Quinto, *Singularities of the X-ray transform and limited data tomography in $\mathbb{R}^2$ and $\mathbb{R}^3$*, SIAM J. Math. Anal., vol. 24, pp 1215-1225, 1993.

[4] A. Faridani et al., *Introduction to Local Tomography*, in Radon Transforms and Tomography, E. T. Quinto et al. (editors), Contemporary Mathematics, Vol. 278, American Mathematical Society, Providence, Rhode Island, pp. 29-47,2001.

[5] A.I. Katsevich and A.G. Ramm, *Pseudolocal tomography*, SIAM J. Appl. Math., 56, N1, pp 167-191, 1996.

[6] D.L. Donoho, *Nonlinear solution of linear inverse problems by wavelet-vaguelette decomposition*, Appl. and Comp. Harm. Anal. 2, pp 101-126, 1995.

[7] E. J. Candès and F. Guo. *New Multiscale Transforms, Minimum Total Variation Synthesis: Applications to Edge-Preserving Image Reconstruction*, Signal Processing. 82, pp 1519–1543, 2002.

[8] C. Berenstein and D. Walnut, *Wavelets and Local Tomography*, in Wavelets in Medicine and Biology, pp 231-261, CRC Press, 1996.

[9] M. Holschneider, *Inverse Radon transforms through inverse wavelet transforms*, Inverse Problems, vol.7, pp 853-861, 1991.

[10] R. Murenzi, *Ondelettes multidimensionnelles et applications à l'analyse d'images*, Thèse, Louvain La Neuve, 1989.

[11] A. Faridani, *Introduction to the Mathematics of Computed Tomography*, Inside Out: Inverse Problems and Applications, G. Uhlmann (editor), MSRI Publications Vol. 47, Cambridge University Press, 2003, pp. 1-46.

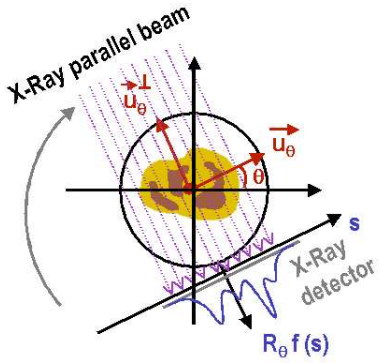

(a) The acquisition and parametrization of the Radon Transform

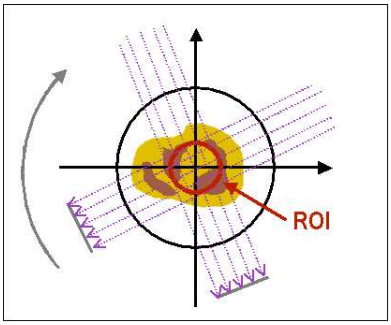

(b) The interior problem : only measures of the Radon Transform across a region of interest are computed.

Fig. 1. The Radon Transform, in case of complete or truncated data.

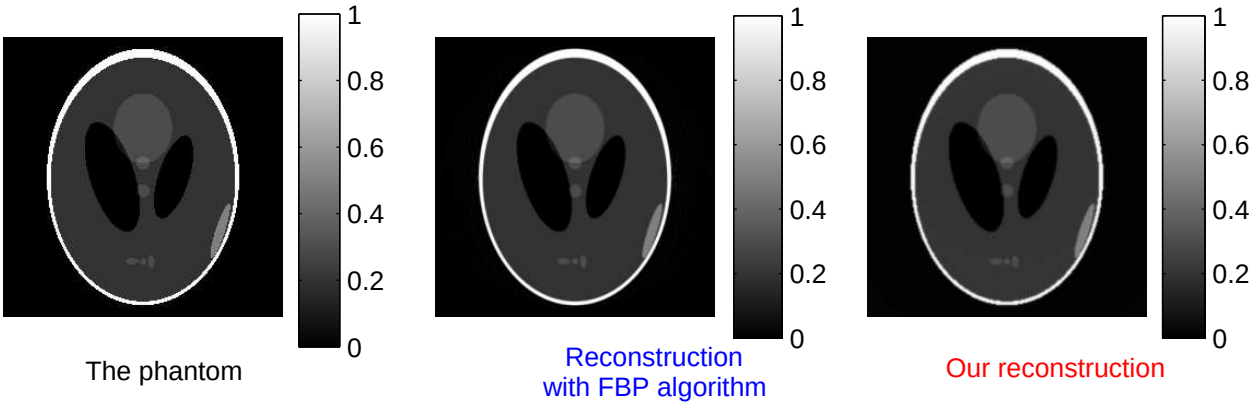

(a) Image reconstruction results

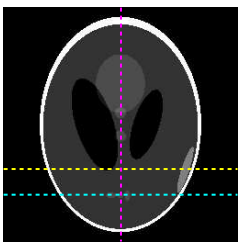

(b) Cross-sections of interest.

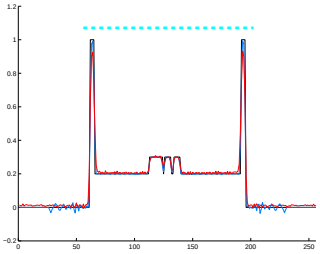

(c) Cross-section 1 (in black: the phantom; in blue: FBP; in red: our method

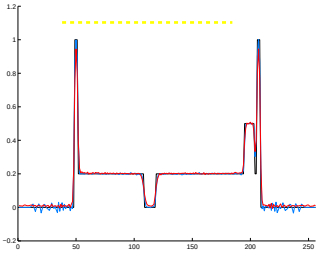

(d) Cross-section 2

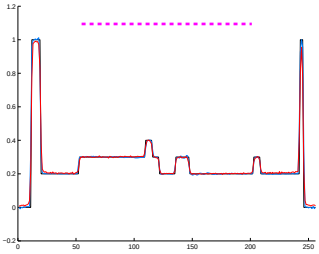

(e) Cross-section 3

Fig. 2. Inversion of the Radon Transform using complete data : image reconstruction and cross-section results

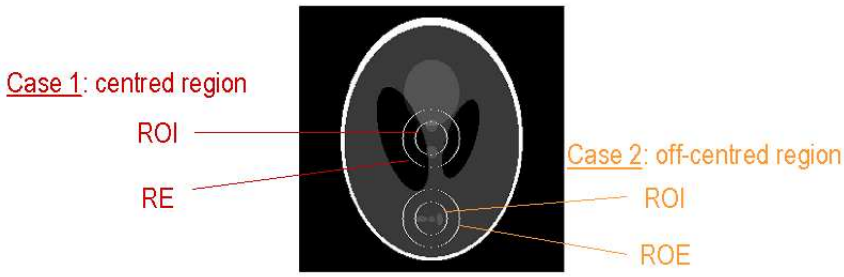

(a) Definition of regions of interest, with associated region of exposition.

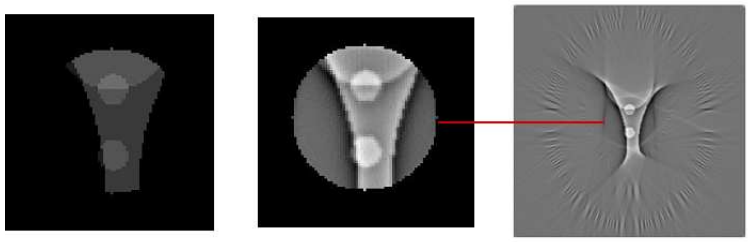

(b) Case 1: the region of interest is centered.

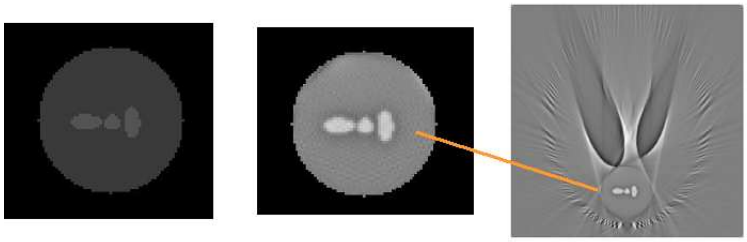

(c) Case 2: the region of interest is off-centered.

Fig. 3. Reconstruction results in two cases of truncated projections. On the left, phantom zooms-in on the region of interest, and on the right, reconstruction results with corresponding zooms-in in the ROI.